American Mineralogist, Volume 92, pages 577–586, 2007

The effect of valence state and site geometry on Ti $L_{3,2}$ and O K electron energy-loss spectra of Ti_xO_y phases

E. Stoyanov,[1,2,*] F. Langenhorst,[1,2] and G. Steinle-Neumann[2]

[1]Institut für Geowissenschaften, Friedrich-Schiller-Universität Jena, Burgweg 11, D-07749 Jena, Germany
[2]Bayerisches Geoinstitut, Universität Bayreuth, D-95440 Bayreuth, Germany

Abstract

Titanium $L_{3,2}$ and O K electron energy loss near-edge structures (ELNES) of seven Ti oxides have been measured in a transmission electron microscope to obtain information on the valence state and site geometry of Ti. The coordination of Ti in all phases studied is octahedral, whereas the valence states occurring are Ti^{2+}, Ti^{3+}, and Ti^{4+}. Effects of polyhedra distortions are particularly observed for two oxides with mixed Ti^{3+}-Ti^{4+} valence state, i.e., the Magnéli phases Ti_4O_7 and Ti_5O_9. A prominent pre-peak in the Ti L_3 edge is attributed to the orthorhombic polyhedra distortions in these compounds, leading to complex crystal field splitting. The effect of valence state manifests itself in a systematic chemical shift of Ti white lines by 2 eV per valence state. On the basis of collected Ti $L_{3,2}$ ELNES spectra we propose a new quantification technique for the determination of Ti^{4+}/Ti^{3+} ratios. Complementary O K ELNES spectra were well reproduced by Density Functional Theory calculation, revealing that the O K-edge is sensitive to the covalent bonding in all analyzed oxides.

Keywords: Electron energy loss spectroscopy, valence state of titanium, titanium oxides, density functional theory

Introduction

Electron energy loss spectroscopy (EELS) is a powerful technique for the detection of valence state, coordination, and site geometry of transition metals in solids. In comparison to the analogous X-ray technique—X-ray absorption spectroscopy (XAS)—the major advantage of EELS is that the spectral data can be obtained with high lateral resolution at the nanoscale. The information on valence state and the local environment of transition metals is then derived from the spectral analysis of the ionization processes resulting from the interaction of an incident electron beam with the solid. The ejection of electrons from inner or core shells (K, L, M, etc.) of atoms in a sample requires that the core electron receive a minimal (critical) ionization energy, E_c, that is a chemical fingerprint of the specific atom and its specific electron shell. In EELS spectra, the minimal ionization energy E_c marks the onset of the ionization edges, which are characterized by a fine structure, the so-called energy-loss near edge structure (ELNES). The ELNES provides a wealth of information about the electronic and atomic structure of solids. In general, the $L_{3,2}$ edges of the 3d transition metals contain information about the valence state, coordination and site symmetry of the central atom. The L_3 edge originates from electron transitions from the inner $2p_{3/2}$ orbitals to empty 3d orbitals of the metal and the L_2 edge originates from $2p_{1/2} \rightarrow 3d$ electron transitions. In the case of Ti oxides, the near-edge structures found in the $L_{3,2}$ edges mainly reflect the covalent bonding states resulting from direct and/or indirect interactions between O and Ti atoms.

Historically, several steps led to an understanding of the electronic information contained in Ti $L_{3,2}$ spectra of oxidic compounds. Fischer (1970) studied $L_{3,2}$ emission and absorption spectra of Ti and V compounds and assigned specific electronic transitions to the spectral features. Leapman et al. (1982) measured $L_{3,2}$ edges of transition metal oxides and compared them to single particle calculations. For the first time, they noticed the unexpected L_3-to-L_2 white line intensity ratio of 0.8:1, which considerably deviates from the statistically expected 2:1 ratio. Brydson et al. (1987, 1989) used the EELS technique to analyze anatase and rutile in great detail. Both ground-state and dynamic Jahn-Teller effects were taken into account to reasonably model Ti K and O K spectra from a quasi-atomic viewpoint. de Groot (1994) revealed the sensitivity of Ti $L_{3,2}$ X-ray absorption spectra of minerals to tetragonal and trigonal distortions of structural polyhedra. At the time, it was demonstrated that the ELNES technique could be used as a fingerprint of the valence state of transition metals in various minerals (de Groot et al. 1992; Garvie et al. 1994). Recent instrumental improvements aided in the measurement of the ELNES of 3d transition metal oxides with an increased spectral resolution of 0.15 eV (Mitterbauer et al. 2003). Despite all these improvements in the measurement and interpretation of Ti $L_{3,2}$ spectra there is however still no attempt to quantify the spectral information in terms of, e.g., the valence state. This paper is therefore aimed at addressing the problem of quantifying the spectral Ti data.

A second issue of this study is to assess the complementary information contained in O K-edge spectra of titanium compounds. It is well known that the transition-metal oxides are not purely ionic and have strong covalent contributions (Owen and Thornley 1966; Sugano et al. 1970). Therefore, studying the O K ELNES can reveal the degree of covalency in the analyzed Ti oxides.

* E-mail: emil.stoyanov@uni-bayreuth.de

0003-004X/07/0004–577$05.00/DOI: 10.2138/am.2007.2344

The O K ELNES spectra of half of the 3d transition metals are interpreted by Grunes et al. (1982), using an extended Hueckel tight-bonding band structure calculation. In these calculations, the first two unoccupied-band DOS peaks of rutile agree well with the experimental separation of the first two fine-structure peaks in the O K, Ti K, and Ti $L_{3,2}$ edges. Furthermore, first principles molecular calculations by Yoshiya et al. (1999) provided sophisticated explanations for the chemical shifts in O K spectra of three Ti oxides. Systematic O K-edge measurements of rutile, anatase, brookite, ilmenite, and perovskite have led to a subdivision of spectra into two regions (Brydson et al. 1992): (1) The onset of O K spectra is interpreted to result from interaction of the hybridized oxygen 2p orbitals with titanium 3d orbitals. (2) At higher energy losses from oxygen 2p to titanium 4s and 4p orbitals occur. In the case of perovskites, Brydson et al. (1992) suggested that the O K ELNES of oxygen in linear twofold coordination might be used as a fingerprint.

The third aspect of this paper deals with the calculation of ELNES spectra of Ti compounds. Although the ELNES is directly related to the details of the electronic structure of the solids, interpretation of particular features in the experimental spectra is not always straightforward and thus modeling of EELS spectra is essentially required. The modeling techniques are mainly divided into two groups: (1) multiple scattering (MS) and (2) first principles calculations on the basis of Density Functional Theory (DFT). MS calculations are based on the interpretation of ELNES as multiple scattering event of the outgoing electron wave by atomic shells around the excited atom. MS calculations and the multiplet effects for Ti-bearing compounds are well studied in several papers by de Groot et al. (1990a, 1990b), de Groot (1994, 2001, 2005), and Wu et al. (2002). For example, the latter authors measured O K-edges of a series of Ti-bearing compounds and demonstrated good agreement between experimental spectra and MS computed O K-edges. DFT solves the Kohn-Sham equations (Schrödinger like wave equations) for the ground state charge density. DFT computations in the linearized augmented plane wave (LAPW) implementation have proven to provide quantitative information about the extended fine structure region of metal atoms (Rez et al. 1999). In this paper, we will hence follow up this approach in computing O K-edge spectra.

Overall, our study is aimed at determining the valence state and site geometry of Ti in minerals at the nanometer scale, using EELS. To achieve this goal, Ti $L_{3,2}$ and O K spectra of seven Ti oxides have been measured with Ti valence states of 4+, 3+, and 2+. In the compounds studied here the number of the titanium valence electrons changes from no d-electrons (Ti^{4+}, rutile, and anatase) to 1 d-electron (Ti^{3+}, Ti_2O_3) and 2 d-electrons (Ti^{2+}, TiO). In addition, we use DFT calculations for correct interpretation of the O K ELNES. On the basis of the collected Ti $L_{3,2}$ ELNES spectra we propose a novel technique for the quantitative determination of Ti^{4+}/Ti^{3+} ratios, applicable to oxide minerals with unknown Ti^{4+}/Ti^{3+} ratio. Ti^{3+} has been detected in lunar and meteoritic rocks (Brearley 1993) and can also be expected in the Earth's mantle (McCammon 2005). The knowledge of Ti^{4+}/Ti^{3+} ratios is hence particularly important for understanding the incorporation, element partitioning, and oxidation state in the Earth's mantle and other rocky solar system bodies (Papike et al. 2005). In addition, the knowledge of the Ti site symmetry and coordination in minerals can provide fundamental information on cation ordering and defect clustering in oxidic compounds such as oxygen vacancy ordering in perovskites. It will be shown here how the chemical bonding and site symmetry of the Ti and O and the valence state of titanium influence the shape of the Ti $L_{3,2}$ and O K ELNES.

METHODS

Samples and preparation

In the present study we have analyzed seven Ti oxides with different valence state and site geometry of the titanium: TiO (Ti^{2+}; cubic), Ti_2O_3 (Ti^{3+}), Ti_3O_5 (Ti^{4+}:Ti^{3+} = 1:2), Ti_4O_7 (Ti^{4+}:Ti^{3+} = 1:1), Ti_5O_9 (Ti^{4+}:Ti^{3+} = 3:2), and TiO_2 (Ti^{4+}; rutile and anatase). In all oxides, the titanium is octahedrally coordinated. The Ti^{4+}-bearing phases are widespread natural minerals, whereas phases with lower valence state are rarely reported. The TiO phase, named hongquiite, has only been found in one locality in China (Yu et al. 1974). The Ti_3O_5, Ti_4O_7, and Ti_5O_9 phases are found as rare accessories in meteorites such as chondrites and ureilites (Brearley 1993). Due to the scarcity of these compounds we have used synthetic samples of the low valence state phases.

The cubic TiO sample was prepared by annealing a fine powder of monoclinic TiO at high temperature and pressure, as described by Bartkowski et al. (1997). The starting material was subjected to a pressure of 8 GPa and was then annealed at 1665 °C for 1 min using a multi-anvil apparatus. The sample was then quenched to room temperature at a rate in excess of 200 °C/min at approximately constant pressure. Afterward, the pressure was released over a period of several hours.

The Ti_2O_3 (100 mesh, 99.9%, Aldrich Co.), Ti_3O_5 (2–3 mm long crystals, 99.9%, Johnson Matthey GmbH), and TiO_2 anatase (1–2 µm 99.9%, Johnson Matthey GmbH) samples were standard trade chemical compounds.

Polycrystalline samples of Ti_4O_7 and Ti_5O_9 were synthesized by heating finely ground, compacted mixtures in stoichiometric proportions of TiO_2 (rutile; 2 µm, 99+% Johnson Matthey GmbH) and Ti metal powder (325 mesh, 99%, Johnson Matthey GmbH) in an evacuated (10^{-6} mbar) silica tube at 1150 °C for 1 week, as previously described for Ti_4O_7 by Acha et al. (2003). We used a natural sample of rutile (TiO_2) in pyrope quartzite, which was taken at the classical outcrop at Pirigi (Case Ramelano, Dora Maira Massif, Italy).

For transmission electron microscope (TEM) study, TiO_2, TiO (cubic), Ti_3O_5, and Ti_4O_7 solid specimens were polished into 30 µm thin sections. They were mounted on copper or molybdenum grids and then thinned by Argon ion beam bombardment in a Gatan Duomill ion-milling machine (4.5 kV, 1 mA). The anatase and Ti_2O_3 samples were crushed in a mortar, suspended in alcohol and then deposited on 3 mm copper grids coated with a holey amorphous carbon film.

Transmission electron microscopy and electron energy-loss spectroscopy

The so-prepared specimens were then studied in an analytical Philips CM20 FEG (field emission gun) scanning TEM at the Bayerisches Geoinstitut, Germany, operating at 200 kV. The synthesis products (cubic TiO, Ti_4O_7, and Ti_5O_9) were inspected by electron diffraction and high-resolution TEM (HRTEM) to test the quality of crystals and to exclude defects such as crystallographic shear planes that would indicate lateral variations in the valence state (Putnis 1992). Only two compounds (TiO and Ti_3O_5) show lattice defects that however have no influence on the valence state. Due to deformation in the multi-anvil press the cubic TiO contains dislocations in a density of 1×10^{10} m^2. As a consequence of the pseudo-orthorhombic cell dimensions the monoclinic Ti_3O_5 developed numerous growth twins during synthesis (Fig. 1).

ELNES spectra were collected with a Gatan PEELS 666 parallel electron spectrometer attached to the Philips CM20 FEG STEM. The energy resolution of the Schottky field-emitter, defined as the full width at half-maximum height of the zero-loss peak, was between 0.75 and 0.85 eV. The relative sample thickness t/λ, as estimated from the low-loss spectra, was between 0.2–0.8 and the spectra were collected from area of about 70–100 nm in diameter. To ensure that EELS measurements are not dependent on sample orientation, all spectra were collected in diffraction mode far away from zone axes with a relatively large illumination semiangle $\alpha = 8.0$ mrad. To obtain high-energy resolution at good counting statistics, the collection semiangle β and the entrance aperture were chosen to be 1.45 mrad and 2 mm, respectively. Measurements were performed under the following conditions: 0.05 eV/channel and an integration time t = 5–10 s per read-out for

the Ti $L_{3,2}$ edges and 0.1 eV/channel and integration time t = 5–10 s per read-out for the O K-edge. Afterward, the collected spectra were corrected for dark current and channel-to-channel gain variation. An inverse power law background was subtracted, and finally the plural scattering contributions were removed using the Fourier-ratio deconvolution technique. For the calibration of energy scale, the C K-edge of amorphous carbon was measured simultaneously at an energy dispersion of 0.3 eV/channel. To determine the energy positions with a precision of 0.1 eV, numerous measurements were undertaken and averaged. The π* peak of the C K-edge at 285 eV served as fix point for the calibration. This procedure ensures that the energy scales of Ti $L_{3,2}$ and O K spectra for the different samples are not shifted relative to each other.

To remove the continuum contribution from the white line intensities and therefore to obtain pure information on the valence state, we have used the following double arctan-function:

$$f(\Delta E) = \frac{h}{\pi}\left[\arctan\left(\frac{\pi}{w_1}(\Delta E - E_1)\right) + \frac{\pi}{2}\right] + \frac{h}{\pi}\left[\arctan\left(\frac{\pi}{w_2}(\Delta E - E_2)\right) + \frac{\pi}{2}\right], \quad (1)$$

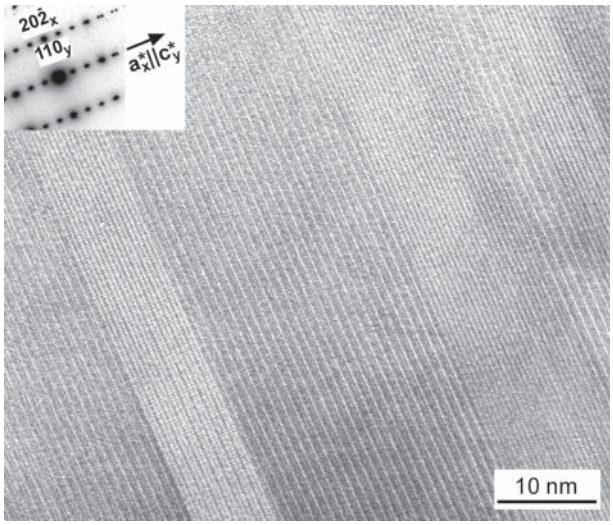

FIGURE 1. High-resolution TEM image of a Ti_3O_5 crystal showing multiple twinning.

where $h = (h_2 - h_1)/2$ is the height of each arctan function with h_1 and h_2 being the heights just before the L_3 and behind the L_2 white lines, respectively. The height h of the two-step functions was chosen to be equal because the intensities of L_3 and L_2 white lines are similar, as well. This is in accordance with previous findings of Leapman et al. (1982), who reported an L_3-to-L_2 intensity ratio of 0.8:1. The widths of the function w_1 and w_2 are fixed to 2 eV. The inflection points E_1 and E_2 were fixed at 457.5 and 463.0 eV, respectively.

Density-of-states calculations

Computations of energy loss spectra within DFT are readily performed by methods that allow the evaluation of the projected densities of states. Well suited are methods that already work with a localized basis such as spherical harmonics. Here we compute the band structure of the Ti oxides by means of the state-of-the-art all electron LAPW method, as implemented in the Wien2k package (Blaha et al. 2001), using the generalized gradient approach (GGA) to the exchange and correlation potential (Perdew et al. 1996). Computations are performed for experimentally determined equilibrium lattice constants and atomic positions. Electronic densities of state are well converged with respect to reciprocal space integration (k-points) and size of the basis set. For the size of the basis set we use a RKmax (i.e., the product of the smallest muffin tin radius in the system and the length of the maximum k-vector of the interstitial plane wave basis) of 7.0. The cross sections were computed from the density-of-states according to the method by Nelhiebel et al. (1999). Here we did not consider the orientation dependence of EELS, but averaged over all possible directions of the scattering vector with respect to the crystal.

However, DFT computations can provide limited information on electron loss processes, as they implicitly assume single electron processes, with one electron being excited from a core to a valence band. This approximation works well for K-edges, whereas for the other edges, in particular the Ti $L_{3,2}$ edges studied here, the agreement is poor. The reason for this discrepancy is the strong overlap of core with valence wave functions that lead to X-ray absorption processes that do not only involve the density-of-states (de Groot 2005).

CRYSTAL STRUCTURES OF TI OXIDES

Basic knowledge of the crystal structures is essentially required for the subsequent interpretation of ELNES spectra. Therefore we briefly review here the crystal structures of the analyzed Ti-oxides (Fig. 2). In all compounds Ti is in octahedral coordination but the polyhedra show variable distortion.

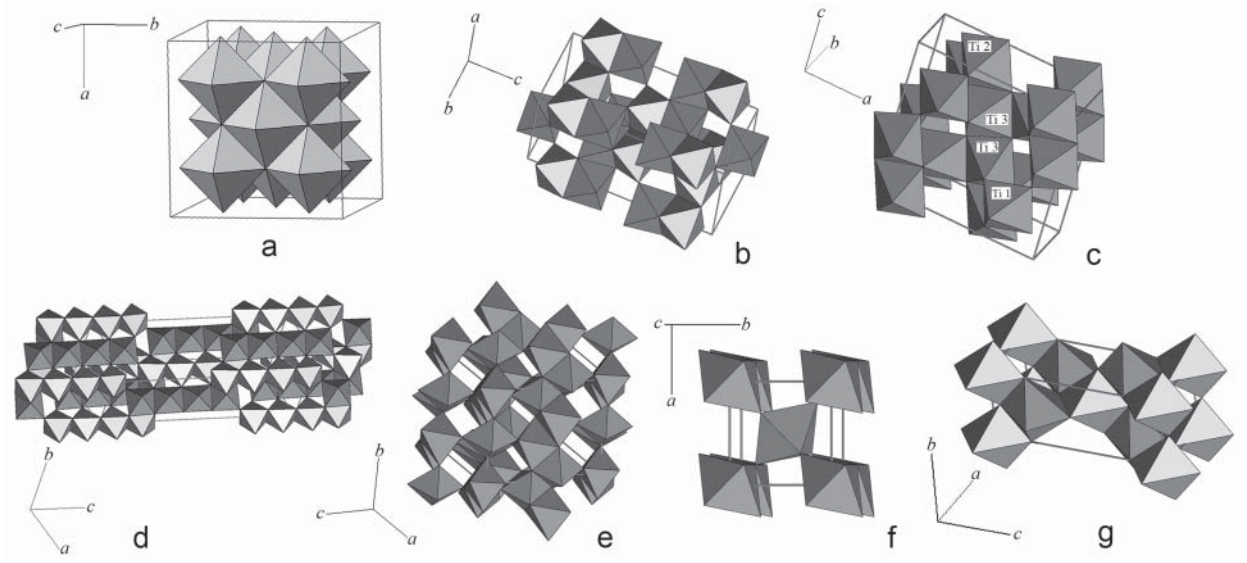

FIGURE 2. Crystal structures of the analyzed oxides: **a** = TiO ($Fm\bar{3}m$), **b** = Ti_2O_3 ($R\bar{3}c$), **c** = Ti_3O_5 ($C2/m$); **d** = Ti_4O_7 ($I\bar{1}$); **e** = Ti_5O_9 ($P\bar{1}$), **f** = TiO_2 (rutile, $P4_2/mnm$), **g** = TiO_2 (anatase, $I4_1/amd$).

TiO (Fig. 2a) has a defective NaCl structure (space group $Fm\bar{3}m$) with equal numbers of randomly distributed vacancies on the cation and anion positions (Wells 1984). Ti_2O_3 has corundum structure (space group $R\bar{3}c$) (Fig. 2b).

The crystal structure of Ti_3O_5 (Fig. 2c) is monoclinic with space group $C2/m$. The Ti atoms in Ti_3O_5 are octahedrally surrounded by O atoms and are located at three crystallographically different sites. The TiO_6 octahedra are linked by sharing edges and corners to form an infinite three-dimensional framework. Characteristic rows of six edge-sharing octahedra persist along the $[\bar{1}03]$ direction. The row is linked to the nearest two rows by sharing three edges in the *ac* plane; its extension along the *b* axis is realized by corner-sharing octahedra.

The oxides Ti_4O_7 and Ti_5O_9 (space groups $I\bar{1}$ and $P\bar{1}$ and Figs. 2d and 2e, respectively) are members of the homologous series Ti_nO_{2n-1} (so-called Magnéli phases). Both phases are mixed valence state oxides, whereby Ti_4O_7 has equal numbers of Ti^{4+} ($3d^0$) and Ti^{3+} ($3d^1$) positions. In the Ti_5O_9 structure the ratio of Ti^{4+} ($3d^0$):Ti^{3+} ($3d^1$) positions is 3:2. The structures of these oxides are similar to that of rutile because they contain rutile-like blocks, which are infinite in *x* and *y* dimensions and are *n* TiO_6 octahedra wide along the *z* dimension ($n = 4$ for Ti_4O_7 and $n = 5$ for Ti_5O_9). This finite dimension is perpendicular to the O-deficient {121} planes of the pseudorutile lattice. These planes are called crystallographic shear planes or Wadsley defects (Putnis 1992). Along the crystallographic shear planes the octahedra share faces, edges, and corners, whereas inside the rutile blocks they share only edges and corners (Marezio et al. 1977; Matsushima and Iguchi 1986).

Both TiO_2 modifications rutile (Fig. 2f) and anatase (Fig. 2g) are tetragonal with space groups $P4_2/mnm$ and $I4_1/amd$, respectively. The symmetry group, number of the coordination polyhedra and the distortion of the polyhedra for the analyzed oxides are given in Table 1.

Figure 3 shows the valence state of Ti in the Ti oxides as function of the volume of the coordination octahedra. Generally, the octahedral volume increases with decreasing

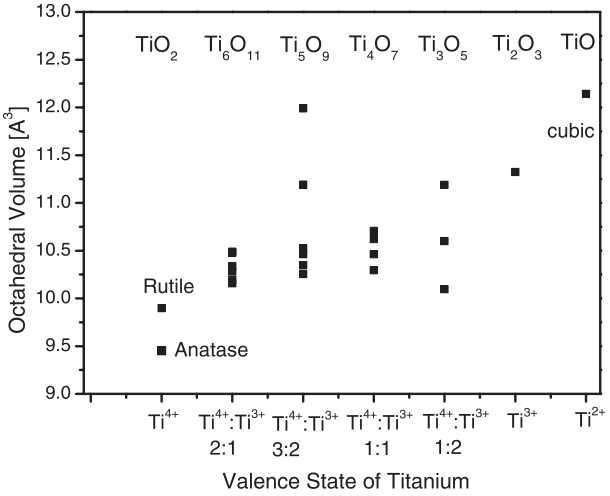

FIGURE 3. Relationship between the valence state of the Ti and the octahedral volume in the analyzed Ti oxides. The octahedral volumes are calculated with PROGRAM METRIC Ver. 6.1 developed by Bartelmehs, Boisen, Gibbs, and Downs (2002), implemented in XtalDraw crystal structure drawing software.

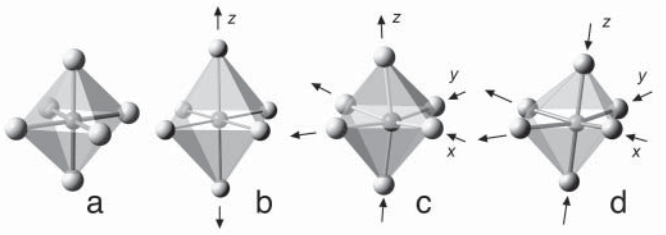

FIGURE 4. Different types of octahedral distortions: **a** = no distortion (cubic TiO), **b** = tetragonal distortion (rutile), **c** = trigonal distortion (Ti_2O_3), **d** = orthorhombic-like distortion (Ti_4O_7 and Ti_5O_9).

TABLE 1. Crystal chemical data for Ti oxides

Compound	Space Group	Ti coordination	Ti valence state	Site symmetry of Ti	Site symmetry of O	Number of the coordination octahedra	Distortion of coordination octahedra
TiO_2 rutile	$P4_2/mnm$	$^{[6]}$Ti	Ti^{4+}	D_{2h}	C_{2v}	1	Ti1 1.0082
TiO_2 anatase	$I4_1/amd$	$^{[6]}$Ti	Ti^{4+}	D_{2d}	C_{2v}	1	Ti1 1.0296
Ti_5O_9	$P\bar{1}$	$^{[6]}$Ti	Ti^{4+}:Ti^{3+} 3:2	C_1, C_i	C_1	6	Ti1 1.0081 Ti2 1.0093 Ti3 1.0203 Ti4 1.0154 Ti5 1.0042 Ti6 1.0091
Ti_4O_7	$I\bar{1}$	$^{[6]}$Ti	Ti^{4+}:Ti^{3+} 1:1	C_1	C_1	4	Ti1 1.0063 Ti2 1.0326 Ti3 1.0120 Ti4 1.0298
Ti_3O_5	$C2/m$	$^{[6]}$Ti	Ti^{4+}:Ti^{3+} 1:2	C_s	C_s	3	Ti1 1.0250 Ti2 1.0268 Ti3 1.0236
Ti_2O_3	$R\bar{3}cH$	$^{[6]}$Ti	Ti^{3+}	C_{3i}	C_2	1	Ti1 1.0086
TiO	$Fm3m$	$^{[6]}$Ti	Ti^{2+}	O_h	O_h	1	Ti1 1.0000

Notes: The distortion of coordination polyhedra is calculated using the following formula (Robinson et al. 1971): $\langle\lambda\rangle = \sum_{i=1}^{n}(l_i/l_0)^2/n$,

where $n = 6$ for O_h symmetry and l_0 = center to vertex distance for a regular octahedron whose volume is equal to that of the undistorted octahedron with bond length l_i.

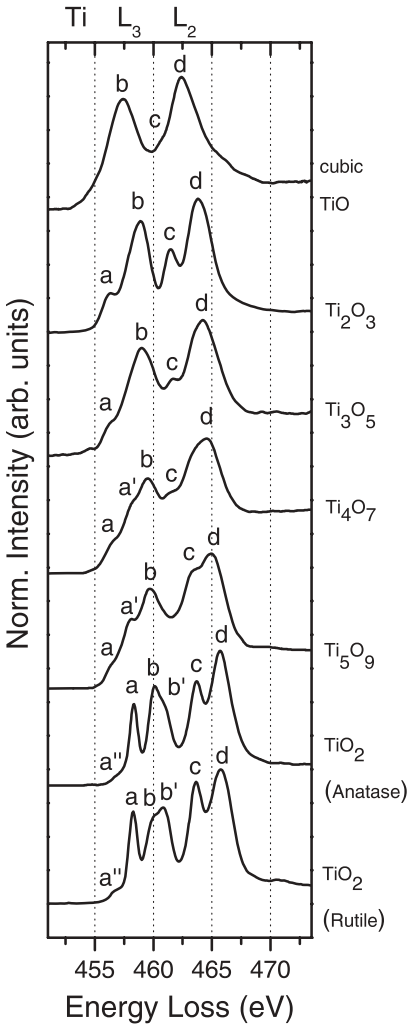

FIGURE 5. Ti $L_{3,2}$ ELNES spectra of the analyzed Ti oxides. The valence state of Ti decreases from the bottom to the top.

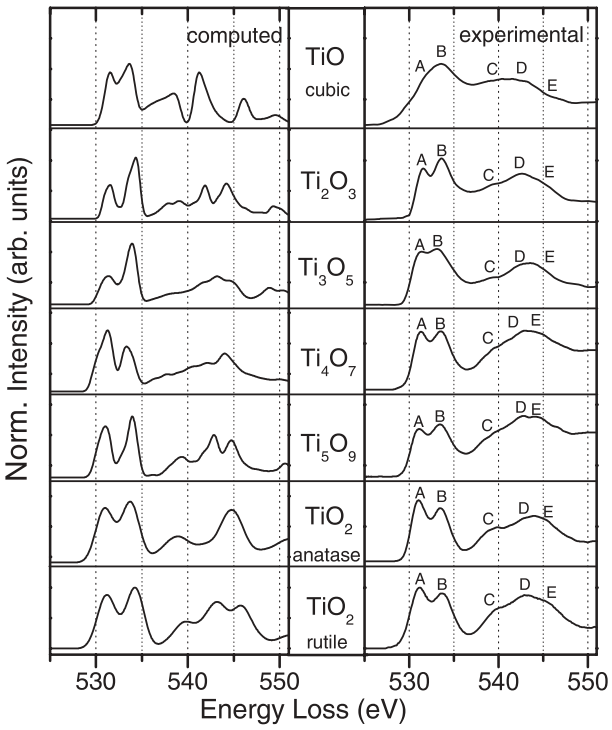

FIGURE 6. Experimental EELS O K-edges and computed oxygen spectra of the various Ti oxides. Note that the computed O K EELS are referenced to energy loss.

valence state. In some of the oxide structures, there are more than just one type of octahedra, with different volumes.

In addition, the site symmetry of the Ti and O atoms in the analyzed oxides differs. The Ti atoms in all oxides except TiO are surrounded by 6 O atoms, and each O atom is surrounded by 3 Ti atoms. In the TiO_2 structure, both the Ti and O atoms are octahedrally coordinated, and the symmetry of the coordination polyhedron is O_h (Fig. 4a). In the rutile structure, the site symmetry of the Ti is D_{2h}, instead of the expected octahedral O_h symmetry. The elongation of O-Ti-O bonds along the z direction of the coordination polyhedron and deviation of the angles from 90° lead to a decrease in symmetry from octahedral to tetragonal D_{2h} symmetry (Fig. 4b). In the case of anatase, the site symmetry of the Ti is D_{2d}, and the symmetry of the coordination polyhedron is also lowered to tetragonal. The O atoms in the rutile and anatase structures lie in a planar unit with site symmetry of C_{2v} (Brydson et al. 1992). In the Ti_2O_3 structure the site symmetry of the Ti is C_{3i}, which leads to the distortion of the coordination polyhedra from octahedral to trigonal symmetry (Fig. 4c). The site symmetry of the O in the Ti_2O_3 structure is reduced to 2. In the Ti_3O_5 the symmetry of both Ti and O atoms is C_s. The Ti and O atoms in the Magnéli phases Ti_4O_7 and Ti_5O_9 are at positions with symmetry 1 (C_1). Andersson and co-workers (Andersson 1960; Andersson and Jahnberg 1963) have shown that only the Ti atoms labeled Ti5 and Ti6 in the Ti_5O_9 structure are located at centers of symmetry (C_i). Finally, a careful investigation of the oxygen polyhedra about the Ti atoms at positions Ti5, Ti2, and Ti6 in the Ti_5O_9 phase shows that they possess orthorhombic-like distortions (Fig. 4d).

RESULTS

Ti $L_{3,2}$ ELNES spectra consist mainly of four white lines labeled a, b, c, and d (two doublets, Fig. 5). The first doublet at lower energy loss comprises the Ti L_3 edge and the second one at higher energy loss the Ti L_2 edge. The two doublets can be further split, whereby the number of the additional peaks depends on valence state, coordination and site symmetry of the Ti atoms (Leapman et al. 1982; Brydson et al. 1989; Garvie et al. 1994).

In the case of the pure Ti^{4+} bearing phases rutile and anatase an additional pre-peak a" appears just in front of the first L_3 peak and the second white line of the L_3 edge is split into peaks b and b'. The Ti L_3 ELNES spectra of mixed valence state compounds Ti_4O_7 and Ti_5O_9 exhibit a splitting of the first white line of the L_3 edge into peaks a and a'. The spectrum of the pure Ti^{3+} oxide (Ti_2O_3) does not display any additional peaks but it is noteworthy that the first white lines in the L_3 and L_2 edges are distinctly less

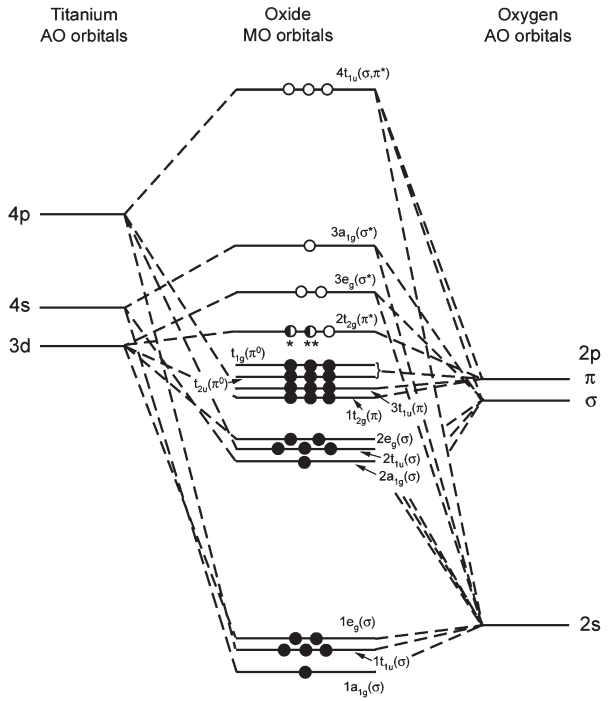

FIGURE 7. Molecular-orbital diagram for rutile and anatase (no electrons on $2t_{2g}$ level), Ti_2O_3 = one electron on $2t_{2g}$ level (half-solid circle *), and TiO = two electrons on $2t_{2g}$ level (half-solid circle **). Modified after Fischer (1970).

TABLE 2. Comparison of the experimentally determined energy positions of the peaks *a*, *a′*, *b*, and *b′* within L_3 edges of Ti oxides

Oxide	Ti L_3 edge peak positions (eV)			
	a	*a′*	*b*	*b′*
TiO_2 rutile	458.3	–	460.0	460.8
TiO_2 anatase	458.3	–	460.0	460.7
Ti_3O_5	456.4	–	459.0	–
Ti_4O_7	456.6	–	459.5	–
Ti_5O_9	456.4	458.2	459.7	–
Ti_2O_3	456.3	458.1	458.9	–
TiO	–	–	457.4	–

TABLE 3. Energy positions of the O *K*-edges in the EELS of the analyzed Ti oxides labeled in Figure 6

Oxide	O *K*-edge peak positions (eV)				
	A	B	C	D	E
TiO_2 rutile	531.1	533.7	~540.0	542.9	~545.6
TiO_2 anatase	531.0	533.5	539.6	543.9	~545.3
Ti_5O_9	531.1	533.3	~539.2	542.7	~544.3
Ti_4O_7	531.3	533.5	~539.4	~542.8	~544.5
Ti_3O_5	531.4	533.2	~539.3	~542.2	~544.9
Ti_2O_3	531.5	533.6	~539.4	542.6	~545.5
TiO	532.0	533.6	~539.7	~542.4	~546.4

intense than the second peaks. This effect is even more pronounced in the EELS spectrum of Ti^{2+} in TiO, showing two main broad L_3 and L_2 white lines preceded by two faint pre-peaks.

A comparison of the obtained Ti $L_{3,2}$ EELS spectra of analyzed Ti oxides reveals that the $L_{3,2}$ onset shifts to lower energy with decreasing oxidation state (Fig. 5). The shift is about 1.7–2.0 eV per oxidation state. The exact energy positions of all identified peaks within the L_3 edge are given in Table 2. These energy positions are in very good agreement with previous measurements of Ti $L_{3,2}$ spectra of anatase, rutile, and Ti_2O_3 (Brydson et al. 1987, 1989; Henderson et al. 2002; Leapman et al. 1982). Only the early data for rutile (Leapman et al. 1982) deviates by a 0.6 eV energy shift from the other data. There are no published data for Ti_3O_5 and both Magnéli phases Ti_4O_7 and Ti_5O_9. Our measurements show that the energy positions of the Ti $L_{3,2}$ peaks of these mixed valence state oxides are in-between those of the end-member Ti^{3+} and Ti^{4+} compounds, as can be expected.

Figure 6 shows a comparison of measured and computed O *K*-edges for the analyzed oxides. The energy positions of the computed O *K* spectra are referenced to energy loss. The features of the experimental and calculated spectra are labeled with A, B, C, D, and E; their energy positions are given in Table 3. The O *K* spectra systematically shift to higher energy losses with decreasing valence state of Ti. Energy positions in the rutile and anatase O *K* ELNES are in good agreement with energies reported by Brydson et al. (1987, 1992) and Grunes et al. (1982). In comparison to our data, the energy positions reported for Ti_2O_3 and TiO (de Groot et al. 1989; Henderson et al. 2003) are shifted by about 0.5–0.6 eV. To our knowledge, the O *K* ELNES of Ti_3O_5, Ti_4O_7 and Ti_5O_9 are presented here for the first time.

DISCUSSION

Interpretation of Ti $L_{3,2}$ ELNES

A useful approach to interpret the Ti $L_{3,2}$ ELNES is to examine and consider the electrical properties of the seven Ti phases. The seven oxides cover a wide variety of electrical properties, reflecting the peculiar electronic structure of each phase. Cubic TiO shows metallic conductivity over a wide range of temperatures (Morin 1959; Bartkowski et al. 1997). Ti_2O_3 has an abrupt semiconductor-to-metal transition below its Neel temperature of 660 K (e.g., Abrahams 1963; Honig and Reed 1968; Rice and Robinson 1976). Ti_3O_5 has metallic conductivity just above 460 K (Bartholomew and Frankl 1969; Onoda 1998). Both Magnéli phases Ti_4O_7 and Ti_5O_9 show semiconductor-to-metal transitions, whereas rutile and anatase (TiO_2) are insulators. Ti_4O_7 has three different phases with phase transitions at 130 and 150 K. The electrons in the high-temperature phase are completely delocalized and the oxide becomes paramagnetic (Abbate et al. 1995). At room temperature Ti_4O_7 has metallic conductivity (Bartholomew and Frankl 1969). Such different electrical properties are due to differences in the degree of occupancy, bond type and the strength of the interactions between the metal 3*d* orbitals and between the metal 3*d* and oxygen 2*p* orbitals.

In EELS, a core hole is created via excitation of a titanium 2*p* electron. At threshold energy this electron is excited to the lower unoccupied 3*d* state. For a pure metal, the transitions at threshold are to the unfilled portion of the conduction band lying just above the Fermi level. After excitation of the core electron, a hole of positive charge is created toward which the remaining one-electron orbitals relax adiabatically (Leapman et al. 1982). The core hole is well screened by relaxation of the other conduction electrons and the distribution of valence electrons is similar to the ground state.

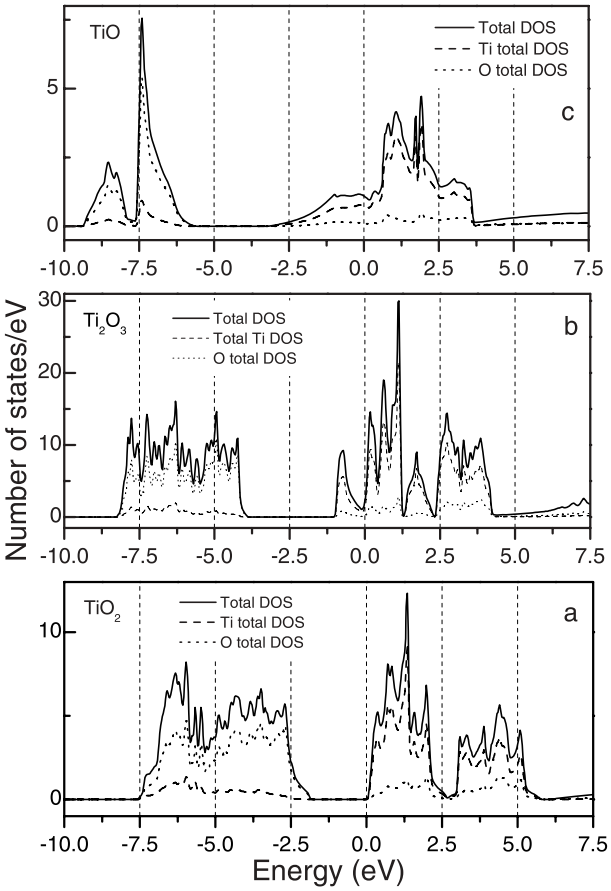

FIGURE 8. Calculated titanium 3*d* DOS and oxygen 2*p* DOS in three Ti-oxides: **a** = TiO_2 (rutile); **b** = Ti_2O_3, **c** = TiO.

The analyzed oxides are semi-conductors or insulators (except TiO) and the formed core hole is incompletely screened from the excited electron. In the case of rutile (insulator) there are no electrons on the first unoccupied $2t_{2g}$ level (Fig. 7), the screening is poorest and the $L_{3,2}$ edges are shifted to higher energy losses than for metallic Ti. In the case of the semi-conducting oxides (Ti_3O_5, Ti_2O_3, Ti_4O_7, and Ti_5O_9) the screening of the 2*p* hole is better and the Ti $L_{3,2}$ edges are shifted closer to the edge of metallic Ti with the L_3 edge at 456 eV and the L_2 edge at 462 eV. TiO shows metallic conductivity and the screening of the created core hole is almost like that in metallic Ti. In this case the Ti L_3 edge is shifted to 456.6 eV.

An alternative approach to explain the chemical shifts in the Ti $L_{3,2}$ spectra of Ti oxides is given by Yoshiya et al. (1999). They performed first principles molecular orbital calculations for three Ti oxides (TiO, Ti_2O_3, TiO_2) and suggest that the Ti-O covalent bonding becomes stronger with decreasing number of d-electrons. To explain the features in the experimental Ti EELS spectra, we apply here this molecular orbital (MO) model. The MO energy-level diagram for the TiO, Ti_2O_3, and TiO_2 phases is shown in Figure 7 and has been adapted from Fischer (1970).

To construct a molecular-orbital energy-level diagram for the Ti oxides it is necessary to consider the titanium 3*d*, 4*s*, and 4*p* atomic orbitals and the oxygen 2*s* and 2*p* orbitals. The zero energy is arbitrarily placed at the Fermi level, which is assumed to be at the partially filled $2t_{2g}$ level in the MO diagram. The interaction between the Ti 3*d* and oxygen 2*p* orbitals rises the $2e_g$, $1t_{2g}$, $2t_{2g}$, and $3e_g$ MO levels, the first two being bonding and the latter two antibonding orbitals (Fischer 1970). The σ bonds are formed from the e_g orbitals, the π bonds from t_{2g} orbitals. There is also an interaction between oxygen 2*p* orbitals with the titanium 4*s* and 4*p* orbitals, which form the $2a_{1g}$, $2t_{1u}$, $3t_{1u}$, $3a_{1g}$, and $4t_{1u}$ MO levels (Grunes et al. 1982; de Groot et al. 1989). The $1a_{1g}$, $1t_{1u}$, and $1e_g$ MO levels are due to some slight interactions between ligand 2*s* and metal 3*d*, 4*s*, and 4*p* orbitals. The t_{2u} and t_{1g} levels are nonbonding oxygen 2*p* lone pairs. All of the Ti oxides have essentially the same MO arrangement. The levels below the $2t_{2g}$ level are completely filled with electrons. The major difference in the electron structure of the main three Ti oxides (TiO, Ti_2O_3, and TiO_2) is the degree of occupancy of the $2t_{2g}$ level. TiO has two $2t_{2g}$ electrons, Ti_2O_3 has one, and TiO_2 has none. This difference is very noticeably reflected in the position of the Ti $L_{3,2}$ edges in the EELS spectra on Figure 5. The Ti $L_{3,2}$ lines are due to the transitions from the inner Ti 2*p* levels to the titanium 3*d* levels. The L_3 edge contains the peak *a* (Fig. 5), which is due to transitions from $2p_{3/2}$ Ti level to the $2t_{2g}$ MO level and the peak *b*, which is due to transitions from the $2p_{3/2}$ Ti level to the $3e_g$ MO level (Leapman et al. 1982).

Interpretation of O *K* ELNES

Oxygen *K* ELNES spectra show several features that are sensitive to the local environment (Fig. 6), i.e., to the variable degree of distortion of the coordination octahedra among the studied Ti oxides. An octahedral ligand field causes the five Ti degenerate *d* states in the conduction band to split into the twofold e_g (d_{z^2} and $d_{x^2-y^2}$ orbitals) and the threefold t_{2g} (d_{xy}, d_{yz}, and d_{xz} orbitals) states. The d_{z^2} and $d_{x^2-y^2}$ orbitals are directed at the ligands, and the d_{xy}, d_{yz}, d_{xz} orbitals are directed between the O atoms.

The experimental spectra (Fig. 6) consist of two main peaks in the energy region between 529 and 535 eV (see Table 3 for exact positions for each oxide). These peaks originate from transitions between oxygen 1*s* and 2*p* σ* states that are hybridized with empty Ti 3*d* orbitals (de Groot et al. 1989). The splitting into two peaks (labeled A and B in Fig. 6) is due to t_{2g}-e_g splitting of the Ti 3*d* levels and the intensity is related to the degree of covalency between the O atoms and the Ti (de Groot et al. 1989). Therefore, peak A is assigned to O $2p \rightarrow$ Ti $3d(t_{2g})$ and B to O $2p \rightarrow$ Ti $3d(e_g)$.

The O *K* ELNES spectra also show a second set of bands in the ~537–546 eV range. These bands are due to transitions from oxygen 2*p* states that are hybridized with Ti 4*s* and 4*p* states (de Groot et al. 1989). The presence of the peaks C, D, and E can be explained with interactions between O 2*p* orbitals and titanium 4*s*/4*p* orbitals (Yoshiya et al. 1999). In addition, in orthorhombic distortion the $4t_{1u}$ level is split into 3 sublevels—$4b_{1u}$, $4b_{3u}$, and $4b_{2u}$. Thus, we may assign the peaks C and D to the lowest unoccupied $4t_{1u}$ bands and the peak E to transitions to higher $4t_{1u}$ type bands. The peaks C, D, and E can alternatively be explained in terms of resonance scattering within shells of neighboring anionic backscatterers. Kurata et al. (1993) use first full multiple-scattering calculations and interpret such spectral features as a result of the arrangement of the O anions around

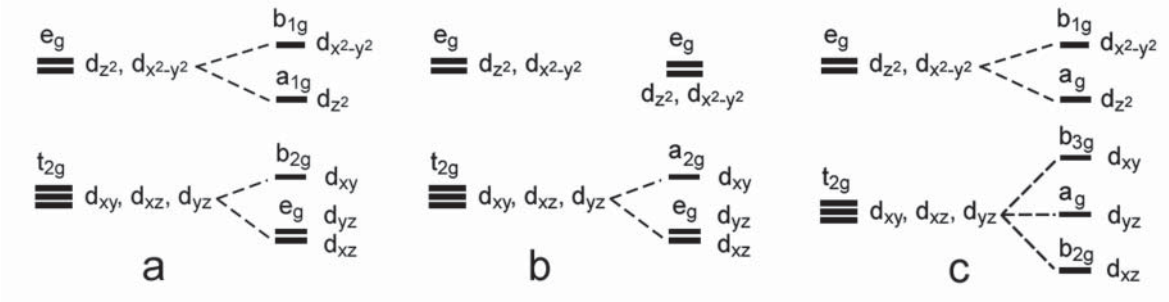

FIGURE 9. Splitting of the t_{2g} and e_g levels in tetragonal (**a**), trigonal (**b**), and orthorhombic (**c**) distorted environments.

the excited central atom.

To extract further information on the electronic structure of the analyzed Ti oxides and to explain the observed features in the O *K* EELS spectra, we performed DFT computations that involved all O electrons. The computations were performed omitting a core hole. Calculated O *K* spectra generally agree well with measured spectra (Fig. 6). We note the following spectral changes as function of increasing valence state: (1) the ligand-field splitting (between peaks A and B) and the energy separation between the Ti 3*d* and Ti 4*s*/4*p* orbitals become larger, and (2) the Ti 4*s*/4*p* band-width decreases. The ligand-field splitting between peaks A and B depends on the magnitude of covalent bonding. As the number of *d* electrons increases from TiO_2 to TiO, covalent bonding between Ti and O becomes ionic. The energy separation between the Ti 3*d* and O 2*p* orbitals increases from TiO_2 to TiO, which results in the smaller bandwidth of Ti 3*d* and thus the resultant conductivity of the oxides (Fig. 8). TiO and Ti_3O_5 possess metallic conductivity and hence show a small A-B splitting of about 1.8–1.9 eV. Due to the semiconductor-to-metal transitions of Ti_2O_3 and both Magnéli phases the splitting of the A-B peaks is about 2.1–2.3 eV. Rutile and anatase are insulators and have consequently an even larger A-B splitting of 2.5 eV.

Effect of site symmetry on Ti $L_{3,2}$ ELNES

The distortions of the octahedral arrangement of central Ti atoms are shown in Table 1. The main distortions in rutile and anatase are the elongation of the O-Ti-O bond in the *c* direction and deviation in the O-Ti-O angles from 90°, which leads to a tetragonal environment and decrease in symmetry of the coordination polyhedra from O_h to D_{2h} and D_{2d}, respectively (de Groot 1992). The features found in the experimental spectra of rutile and anatase are described in great detail by Leapman et al. (1982), Brydson et al. (1989), and de Groot et al. (1990a). For tetragonal coordination of Ti atoms in rutile, Brydson et al. (1989) suggest that a dynamic Jahn-Teller effect raises the splitting of the $2t_{2g}$ and $3e_g$ levels as it is shown in Figure 9a. The distortion affects also the higher energy level $4t_{1u}$, which is split into 3 sublevels—$4b_{1u}$, $4b_{3u}$, and $4b_{2u}$. This splitting influences the O *K*-edge and will be discussed later. The splitting of the Ti 3*d* orbitals allows several electron transitions instead of one in non-distorted octahedra. The measured spectrum exhibits a splitting of the *b* peak. The peak *b*' is due to the split $3e_g$ level. There are no electrons on the $2t_{2g}$ level and this peak can be explained with the preferable ejection of the excited $2p_{3/2}$ electron to the split $3e_g$ level. Gupta and Ellis (1976) performed molecular cluster predictions for rutile structures and pointed out that the splitting of the e_g level is weakly dependent on the angle variation. Our measurements show that the splitting of the $3e_g$ level in both rutile and anatase is about 0.8 eV, which is in good agreement with the previously reported splitting of 0.9 eV (Brydson et al. 1989). The Ti ELNES of rutile exhibits one more additional feature just before the L_3 edge (assigned *a*" in Fig. 5). Because of the dominating $2p \rightarrow 3d$ transitions this peak is unlikely to be assigned to $2p \rightarrow 4s$ transitions, which are much weaker and contribute to the background observed at the higher energies. Brydson et al. (1989) suggest that this peak could be due to excitonic transitions below the band gap. Ogasawara et al. (2001) perform relativistic cluster calculation and suggest that the peak *a*" originates from multiplet splitting of the same electronic configuration as peak *a* $[(2p_{1/2})^2(2p_{3/2})^3(t_{2g})^1(e_g)^0]$. After performing multiplet calculations by de Groot et al. (1990b), the pre-peak *a*" can be attributed to the ^1P multiplet. In addition, Brydson et al. (1993) and Mitterbauer et al. (2003) notice that the pre-peak feature is due to the spin forbidden $p_{3/2}$-$d_{3/2}$ transitions and therefore its intensity is low compared to the main L_3 line.

The trigonal distortion is represented in Ti_2O_3. In this case the t_{2g} level is split into two components, while the e_g level remains

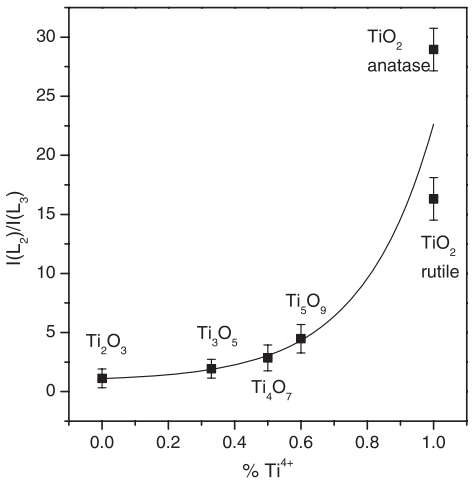

FIGURE 10. Calculated white line intensity ratio $I(L_2)/I(L_3)$ as a function of the Ti^{4+} concentration $Ti^{4+}/\Sigma Ti$.

unchanged (Dionne 2002). A trigonal distortion lowers the symmetry to D_{3d}, and splits the ground t_{2g} state into an a_{2g} and an e_g level (Fig. 9b). The mathematical treatment of this problem was previously provided by Gladney and Swalen (1965) and Englman (1966). In the case of Ti_2O_3, the combination of spin-orbit coupling and trigonal distortion removes the spin microstate degeneracy and leads to zero-field splitting. This can explain the lack of any additional peaks in the Ti_2O_3 spectrum.

The Ti_4O_7 and Ti_5O_9 have triclinic crystal structures and possess a compression of the coordination polyhedron along the z axis and a corresponding elongation of x or y axes. This results in a large deviation of the O-Ti-O angles from 90° and an orthorhombic-like distortion of the polyhedron. Both oxides have mixed Ti valence state and $2t_{2g}$ levels are partially occupied. The ELNES spectra show that, in orthorhombic-like distortions, the t_{2g} level splits at least into two components (see a and a' in Ti_4O_7 and Ti_5O_9 spectra, Fig. 5). Ravikumar et al. (1999) found that the t_{2g} level is split into three components for Cr^{3+} in orthorhombic coordination. For the Magnéli phases, such orthorhombic-like distortions (Fig. 9c) may explain the presence of peak a' that is probably due to ejection of the $2p_{3/2}$ excited electrons to the split t_{2g} level. We found a $2t_{2g}$ level splitting of 1.85 eV for Ti_4O_7 and 1.65 eV for Ti_5O_9. The presence of Ti^{3+} and Ti^{4+} in these two oxides, both in distorted oxygen environments, leads to a broadening of the main four white lines. Both Magnéli phases contain a large number of differently distorted octahedral arrangements (see Table 2), which leads to more complex ELNES spectra. This means that the spectra of Magneli phases well reflect the variable chemical environments of Ti atoms due to different valence states and distorted polyhedra.

Quantification of the valence state of Ti

To obtain quantitative information on the valence state of Ti in oxidic compounds with a mixed valence between Ti^{3+} and Ti^{4+}, we have developed a technique that is based on the calibration of the chemical shift observed in Ti $L_{3,2}$ spectra. The energy positions of spectral features used here for the proposed quantification technique agree very well with previous Ti $L_{3,2}$ edge measurements (Brydson et al. 1987, 1989; Henderson et al. 2002). The method is similar to the universal method for the valence state determination of iron (van Aken et al. 1998) and relates changes in the $I(L_2)/I(L_3)$ intensity ratio to the Ti valence state. Two integration windows of each 1 eV width were applied to the Ti $L_{3,2}$ edges. The windows are centered on the first white line in the L_3 region for Ti^{3+} and the second white line in the L_2 region for Ti^{4+}. They cover the energy regions from 455.8 to 456.8 eV and from 465.25 to 466.25 eV, respectively. The choice of these 1 eV integration windows ensures also that the influence of multiple scattering and multiplet splitting due to polyhedron distortions is suppressed.

In Figure 10, the white line intensity ratio $I(L_2)/I(L_3)$ calculated according to this technique is plotted as a function of $Ti^{4+}/\Sigma Ti$ with $\Sigma Ti = Ti^{4+} + Ti^{3+}$. The values for $I(L_2)/I(L_3)$ ratios range from 1.1177 (Ti_2O_3) to 28.9493 (TiO_2, anatase). The $I(L_2)/I(L_3)$ value for rutile is lower (16.3072) than that for anatase. According to calculations and measurements of Ti $L_{3,2}$ X-ray absorption spectra (Crocombette and Jollet 1994), intensity variations are actually observed in the spectra of the three TiO_2 polymorphs rutile, anatase, and brookite. These intensity variations are attributed to the slight differences in the first coordination shell of the Ti atoms in the three polymorphs. Thus, there is some general uncertainty regarding the calculated $I(L_2)/I(L_3)$ ratio for pure Ti^{4+}-bearing phases.

For empirical fitting of experimental data, we used an average value calculated from the intensity ratios of anatase and rutile. The experimental data shows an exponential relationship that can be best expressed by the following equation:

$$y(x) = y_0 + A_1 e^{\frac{x}{t_1}} \qquad (2)$$

with the fit values $y_0 = 0.87953 \pm 0.19092$, $A_1 = 0.21992 \pm 0.04253$, and $t_1 = 0.21767 \pm 0.00884$. The correlation coefficient R^2 of the fit is 0.99 and $Chi^2/DoF = 0.03$. Using the details from the fit and after simple mathematical transformations we can rewrite the equation above as follows:

$$x = \left[\ln\left(\frac{a - 0.87953}{0.21992}\right)\right] \times 0.21767 \qquad (3)$$

where x is the Ti^{4+} concentration in the sample and a is $I(L_2)/I(L_3)$. Equation 3 can be used for a quantitative determination of $Ti^{4+}/\Sigma Ti$ without knowledge of sample composition or site geometry of the Ti.

The Ti^{4+} calibration method proposed is applicable for total Ti concentrations down to about 1 at%. For lower Ti concentrations the jump ratio (signal/background) becomes very small, i.e., after subtraction of the background the noise dominates the spectrum. The precision of the method strongly depends on the correct determination of the Ti $L_{3,2}$ energy positions. The experimental error for the repeated determination of energy positions is about ±0.1 eV. Taking into account this deviation the calculated error for the $Ti^{4+}/\Sigma Ti$ determination is up to 10%. It is noteworthy that in the case of very low Ti^{3+} concentrations there will be larger uncertainties due to the aforementioned variations in the intensity ratios for various TiO_2 standards. Overall, the proposed quantification technique is capable of yielding reasonable valence state information on Ti. It can be used to obtain important data on the oxidation state and crystal chemistry of minerals as well as on redox reactions taking place in planetary interiors and surfaces.

Acknowledgments

E.S. is grateful to the Bayerisches Geoinstitut (Bayreuth, Germany) where this study has been largely performed, and appreciates the support by the International Graduate School "Oxides" funded under the Elite Program Bavaria. The research project was supported by the Deutsche Forschungsgemeinschaft under the grant LA 830/7-1 (to F. Langenhorst, D. Frost, and G. Steinle-Neumann). We thank the two anonymous reviewers and Hongwu Xu for the constructive corrections. We acknowledge Hubert Schulze for the excellent preparation of numerous TEM thin sections.

References cited

Abbate, M., Potze, R., Sawatzky, G.A., Schlenker, C., Lin, H.J., Tjeng, L.H., Chen, C.T., Teehan, D., and Turner, T.S. (1995) Changes in the electronic structure of Ti_4O_7 across the semiconductor-semiconductor-metal transitions. Physical Review B, 51, 10150–10153.

Abrahams, S.C. (1963) Magnetic and crystal structure of titanium sesquioxide. Physical Review B, 130, 2230–2237.

Acha, C., Monteverde, M., Núñez-Requeiro, M., Kuhn, A., and Alario Franco, M.A. (2003) Electrical resistivity of the Ti_4O_7 Magnéli phase under high pressure. The European Physical Journal B, 34, 421–428 (arXiv:cond-mat/0310048 v1 2 Oct 2003).

Andersson, S. (1960) The crystal structure of Ti_5O_9. Acta Chemica Scandinavica, 14, 1161–1172.

Andersson, S. and Jahnberg, L. (1963) Crystal structure studies on the homologous series $Ti_n O_{2n-1}$ $V_n O_{2n-1}$ $Ti_{n-2} Cr_2 O_{2n-1}$. Acta Chemica Scandinavica, 14, 1161–1172.

Bartholomew, R.F. and Frankl, D.R. (1969) Electrical properties of some titanium oxides. Physical Review, 187, 828–833.

Bartkowski, S., Neumann, M., Kurmaev, E.Z., Fedorenko, V.V., Shamin, S.N., Cherkashenko, V.M., Nemnonov, S.N., Winiarski, A., and Rubie, D.C. (1997) Electronic structure of titanium monoxide. Physical Review B, 56, 10656–10667.

Blaha, P., Schwarz, K., Madsen, G.K.H., Kvasnicka, D., and Luitz, J. (2001) WIEN2k, An Augmented Plane Wave + Local Orbitals Program for Calculating Crystal Properties. Karlheinz Schwarz, Technische Universität Wien, Vienna.

Brearley, A.J. (1993) Occurrence and possible significance of rare Ti oxides (Magnéli phases) in carbonaceous chondrite matrices. Meteoritics, 28, 590–595.

Brydson, R., Williams, B.G., Engel, W., Sauer, H., Zeitler, E., and Thomas, J.M. (1987) Electron energy-loss spectroscopy (EELS) and the electronic structure of titanium dioxide. Solid State Communications, 64, 609–612.

Brydson, R., Sauer, H., Engel, W., Thomas, J.M., Zeitler, E., Kosugi, N., and Koruda, H. (1989) Electron energy loss and X-ray absorption spectroscopy of rutile and anatase: a test of structural sensitivity. Journal of Physics: Condensed Matter, 1, 797–812.

Brydson, R., Sauert, H., Engel, W., and Hofer, F. (1992) Electron energy-loss near-edge structures at the oxygen K edges of titanium (IV) oxygen compounds. Journal of Physics: Condensed Matter, 4, 3429–3437.

Brydson, R., Garvie, L.A.J., Craven, A.J., Sauer, H., Hoferl, F., and Cressey, G. (1993) $L_{2,3}$ edges of tetrahedrally coordinated d^0 transition-metal oxyanions XO_4^{n-}. Journal of Physics: Condensed Matter, 5, 9379–9392.

Crocombette, J.P. and Jollet J.F. (1994) Ti 2*p* X-ray absorption in titanium dioxides (TiO_2): the influence of cation site environment. Journal of Physics: Condensed Matter, 6, 10811–10821.

de Groot, F.M.F. (1994) X-ray absorption and dichroism of transition metals and their compounds. Journal of Electron Spectroscopy and Related Phenomena, 61, 529–622.

——— (2001) High-Resolution X-ray Emission and X-ray Absorption Spectroscopy. Chemical Reviews, 101, 1779–1808.

——— (2005) Multiplet effects in X-ray spectroscopy. Coordination Chemistry Reviews, 249, 31–63.

de Groot, F.M.F., Grioni, M., and Fuggle, J.C. (1989) Oxygen 1*s* X-ray absorption edges of transition-metal oxides. Physical Review B, 40, 5715–5723.

de Groot, F.M.F., Fuggle, J.C., Thole, B.T., and Sawatzky, G.A. (1990a) $L_{3,2}$ X-ray-absorption edges of d^0 compounds: K^+, Ca^{2+}, Sc^{3+} and Ti^{4+} in O_h (octahedral) symmetry. Physical Review B, 41, 928–937.

——— (1990b) 2*p* X-ray absorption of 3*d* transition-metal compounds: An atomic multiplet description including the crystal field. Physical Review B, 42, 5459–5468.

de Groot, F.M.F., Figueiredo, M.O., Basto, M.J., Abbate, M., Petersen, H., and Fuggle, J.C. (1992) 2*p* X-ray absorption of titanium in minerals. Physics and Chemistry of Minerals 19, 140–147.

Dionne, G.F. (2002) Magnetoelastic effects of iron-group ions in exchange fields. Journal of Applied Physics, 91, 7367–7369.

Englman, R. (1966) Covalency effects in trigonal distortions. Journal of Chemical Physics, 45, 3862–3869.

Fischer, D.W. (1970) Molecular-Orbital interpretation of the soft X-ray $L_{3,2}$ emission and absorption spectra from some titanium and vanadium compounds. Journal of Applied Physics, 41, 3561–3569.

Garvie, L.A.J. and Craven, A.J. (1994) Use of electron-energy loss near-edge structure in the study of minerals. Amarican Mineralogist, 79, 411–425.

Gladney, H.M. and Swalen, J.D. (1965) Theory of EPR of Ti^{3+} in trigonal environments. Journal of Chemical Physics, 42 1999–2010.

Grunes, L.A., Leapman, R.D., Wilker, C.N., Hoffman, R., and Kunz, A.B. (1982) Oxygen *K* near-edge fine structure: An electron-energy loss investigation with comparisons to new theory for selected 3*d* transition-metal oxides. Physical Review B, 25, 7157–7173.

Gupta, M. and Ellis, D.E. (1976) Cluster model for lattice distortion effects on electronic structure: VO and VO_2. Physical Review B, 13, 3405–3418.

Henderson, G.S., Liu, X., and Fleet, M.E. (2002) A Ti *L*-edge X-ray absorption study of Ti-silicate glasses. Physics and Chemistry of Minerals, 29, 32–42.

——— (2003) Titanium coordination in silicate glasses investigated using O *K*-edge X-ray absorption spectroscopy. Mineralogical Magazine, 67, 597–607.

Honig, J.M. and Reed, T.B. (1968) Electrical properties of Ti_2O_3 single crystals. Physical Review, 174, 1020–1026.

Kurata, H., Lefevre, E., Colliex, C., and Brydson, R. (1993) Electron energy-loss near-edge structures in the oxygen *K*-edge spectra of transition-metal oxides. Physical Review B, 47, 13763–13768.

Leapman, R.D., Grunes, L.A., and Fejes, P.L. (1982) Study of the $L_{2,3}$ edges in the 3*d* transition metals and their oxides by electron-energy-loss spectroscopy with comparisons to theory. Physical Review B, 26, 614–635.

Marezio, M., Tranqui, D., Lakkis, S., and Schlenker, C. (1977) Phase transitions in Ti_5O_9 single crystals: electrical conductivity, magnetic susceptibility, specific heat, electron paramagnetic resonance, and structural aspects. Physical Review B, 16, 2811–2821.

Matsushima, F. and Iguchi, E. (1986) Lattice energy calculations for Ti_4O_7 using a shell model. Journal of Physics and Chemistry of Solids, 47, 45–53.

McCammon, C. (2005) The paradox of mantle redox. Science, 308, 807–808.

Mitterbauer, C., Kothleitner, G., Grogger, W., Zandbergen, H., Freitag, B., Tiemeijer, P., and Hofer, F. (2003) Electron energy-loss near-edge structures of 3*d* transition metal oxides recorded at high energy resolution. Ultramicroscopy, 96, 469–480.

Morin, F.J. (1959) Oxides which show a metal-to insulator transition at the Neel Temperature. Physical Review Letters, 3, 34–36.

Nelhiebel, M., Louf, P.H., Schattschneider, P., Blaha, P., Schwarz, K., and Jouffrey, B. (1999) Theory of orientation sensitive near-edge fine structure core-level spectroscopy. Physical Review B, 59, 12807–12814.

Ogasawara, K., Iwata, T., Koyama, Y., and Ishii, T. (2001) Relativistic cluster calculation of ligand-field multiplet effects on cation $L_{2,3}$ X-ray-absorption edges of $SrTiO_3$, NiO, and CaF_2. Physical Review B, 64, 115413-1–115413-5.

Onoda, M. (1998) Phase transitions of Ti_3O_5. Journal of Solid State Chemistry, 136, 67–73.

Owen, J. and Thornley, J.H. (1966) Covalent bonding and magnetic properties of transition metal ions. Reports on Progress in Physics, 29, 675–728.

Papike, J.J., Karner, J.M., and Shearer, C.K. (2005) Comparative planetary mineralogy: Valence state partitioning of Cr, Fe, Ti, and V among crystallographic sites in olivine, pyroxene, and spinel from planetary basalts. American Mineralogist, 90, 277–290.

Perdew, J.P., Burke, K., and Ernzerhof, M. (1996) Generalized Gradient Approximation Made Simple. Physical Review Letters, 77, 3865–3868.

Putnis, A. (1992) Introduction to Mineral Sciences, 457 p. Cambridge University Press, U.K.

Ravikumar, R.V.S.S.N., Chandrasekhar, A.V., Rao, S.N., Madhu, N., Reddy, B.J., and Reddy, Y.P. (1999) Orthorhombic Site Symmetry of Cr^{3+} in $ZnNH_4PO_4$ $6H_2O$. Crystals. Crystal Research Technology, 34, 911–914.

Rez, P., Alvarez, J.R., and Pickard, C. (1999) Calculation of near edge structure. Ultramicroscopy, 78, 175–183.

Rice, C.E. and Robinson, W.R. (1976) Structural changes associated with the semiconductor-to-metal transition in Ti_2O_3. Materials Research Bulletin, 11, 1355–1360.

Robinson, K., Gibbs, G.V. and Ribbe, P.H. (1971) Quadratic elongation: a quantitative measure of distortion in coordination polyhedra. Science, 172, 567–570.

Sugano, S., Tanabe, Y., and Kitamura, H. (1970). Multiplets of transition metal ions in crystals. Academic Press, New York.

van Aken, P.A., Liebscher, B., and Styrsa, V.J. (1998) Quantitavie determination of iron oxidation states in minerals using Fe $L_{2,3}$-edge electron energy-loss near edge structure spectroscopy. Physics and Chemistry of Minerals, 25, 323–327.

Wells, A.F. (1984) Structural Inorganic Chemistry, p. 562. Clarendon Press, Oxford.

Wu, Z., Paris, E., Langenhorst, F., and Seifert, F. (2002) Oxygen-metal bonding in Ti-bearing compounds from O 1*s* spectra and ab inition full multiple-scatering calculations. Journal of Synchrotron Radiation, 9, 394–400.

Yoshiya, M., Tanaka, I., Kaneko, K., and Adachi, H. (1999) First principles calculations of chemical shifts in ELNES/NEXAFS of titanium oxides. Journal of Physics: Condensed Matter, 11, 3217–3228.

Yu, T.H., Lin, S.J., Chao, P., Fang, C.S., and Huang, C.S. (1974) A preliminary study of some new minerals of the platinum-group and another associated new one in platinum-bearing intrusions in a region of China. Acta Geologica Sinica, 2, 202–218.

MANUSCRIPT RECEIVED JUNE 9, 2006
MANUSCRIPT ACCEPTED NOVEMBER 14, 2006
MANUSCRIPT HANDLED BY HONGWU XU